Polymer Chemistry

ROYAL SOCIETY OF CHEMISTRY

PAPER

View Article Online
View Journal | View Issue

Cite this: *Polym. Chem.*, 2022, **13**, 58

Well-defined polyacrylamides with AIE properties *via* rapid Cu-mediated living radical polymerization in aqueous solution: thermoresponsive nanoparticles for bioimaging†

Congkai Ma,[a] Ting Han,[b] Niu Niu,[b] Lucas Al-Shok,[a] Spyridon Efstathiou,[a] Daniel Lester,[c] Steven Huband[d] and David Haddleton *[a]

There is a requirement for the development of methods for the preparation of well-controlled polymers with aggregation-induced emission (AIE) properties. This requirement directed this current work towards a robust synthetic route, which would be applicable for preparation in water and the presence of many types of functional groups. Herein, aqueous Cu-mediated living radical polymerization (LRP) has been optimized to provide facile and rapid access to a diverse range of water-soluble AIE polymers at sub-ambient temperatures. Homo-, block and statistical copolymerization all proceeded to a near full monomer conversion (≥99%) within 1 or 2 h and exhibited narrow dispersity, even when DP was targeted up to 1000. This excellent control associated with this polymerisation technique and the high-end group fidelity achieved were further demonstrated by linear first order kinetics and successful *in situ* block copolymerization, respectively. Fine-tuning the monomer sequence and composition of poly(*N*-isopropylacrylamide) (PNIPAM) copolymers allows for different lower critical solution temperature (LCST) and fluorescent thermoresponsive nanoparticles, which spontaneously self-assembled to varying sizes in water as determined by a combination of techniques (DLS, SAXS and TEM). Additionally, the fluorescence intensity was demonstrated to depend on the polymer concentration, architecture of the side chains and temperature. Particularly, PNIPAM-containing polymers were resistant to reduction in thermo-induced emission. The good biocompatibility, photostability and high specificity make them promising candidates as lysosome-specific probes for application in bioimaging.

Received 25th October 2021,
Accepted 30th November 2021

DOI: 10.1039/d1py01432c

rsc.li/polymers

Introduction

Until the concept of aggregation-induced emission (AIE) was coined by Tang and coworkers in 2001,[1] molecular aggregation had been regarded to be detrimental to luminescence due to the aggregation-caused quenching (ACQ) phenomenon. Intriguingly, the AIE effect has revolutionarily demonstrated that aggregation can allow for boosted light emission with an appropriate chemical moiety, contributing potential application in optoelectronics,[2–4] environmental detection and monitoring,[5–7] as well as biomedical areas[8–12] over the last decade. Notably, the expansion of AIE research into polymer science enables the fabrication and synthesis of different functional luminescent materials, which can benefit from the excellent mechanical properties of polymers and ready regulation of their composition, structure, and morphology.[13] To date, the majority of AIE-active polymers have been prepared by click polymerization,[14–17] free radical polymerization,[18] ring-opening polymerization,[19] and polycoupling[20] mediated by one-, two- or multi-component polymerization. This has furnished many complex polymeric materials with high atom economy and diverse structures.[21]

Nevertheless, there is still a requirement to develop facile, robust and rapid synthetic strategies to enable the efficient construction of AIE polymers with monomer sequence control and targeted molecular weights as well as well-defined architectures under mild conditions.[16,17] In particular, given increasing interests in biologically relevant polymers and environmentally benign synthesis, the straightforward preparation of functional, narrow disperse water-soluble AIE poly-

[a]*Department of Chemistry, University of Warwick, Coventry, CV4 7AL, UK. E-mail: d.m.haddleton@warwick.ac.uk*
[b]*Center for AIE Research, College of Materials Science and Engineering, Shenzhen University, Shenzhen, 518060, China*
[c]*Polymer Characterisation Research Technology Platform, University of Warwick, Coventry, CV4 7AL, UK*
[d]*Department of Physics, University of Warwick, Coventry, CV4 7AL, UK*
†Electronic supplementary information (ESI) available. See DOI: 10.1039/d1py01432c

mers as prepared in aqueous media at low temperatures remains considerably challenging. Noteworthy, difficulties associated with accurate exploration of the structure–property relationship (SPR) of AIE polymers with broad molecular weight distributions emphasize the significance of polymers with low dispersity ($Đ$).[16]

Reversible deactivation radical polymerizations (RDRP) and living radical polymerization (LRP), including reversible addition–fragmentation polymerization (RAFT),[22,23] atom-transfer radical polymerization (ATRP)[24] and Cu(0)-mediated reversible deactivation radical polymerization (Cu(0)-RDRP),[25,26] allow for the synthesis of well-defined polymers and (multi)block copolymers with quite sophisticated architectures even in aqueous media.[27] Of these techniques, the use of RAFT has been predominant, especially for polymerization of acrylamides in water and aqueous media.[28,29] Indeed, acrylamides have often been demonstrated to be problematic to be polymerized by traditional ATRP approaches with less control over molecular weights or limited synthesis of block copolymers. Perrier *et al.* reported the multiple block copolymerization of comprising up to four different acrylamide monomers with a degree of polymerization (DP) = 10 for each block using RAFT in both aqueous (70 °C) and organic media (65 °C).[28] In a separate study, the same group presented the production of decablock poly(*N*,*N*-dimethylacrylamide) (PDMA) and homopoly(4-acryloylmorpholine) (PNAM) with a final $Đ \sim 1.15$ after 10 block extensions employing the same technique.[29] However, a prolonged reaction time (24 h) for each block was required in both cases. Of particular relevance to AIE, the majority RDRP to polymerize acrylamides were limited in organic solvents. Zhu *et al.* prepared dual-responsive copolymers with AIE features by incorporating a tetraphenylethylene (TPE)-based monomer with poly(*N*-isopropylacrylamide) (PNIPAM), a well-adopted thermosensitive polymer.[30] The copolymerizations were performed in DMF at 70 °C using the RAFT method for more than 24 h and the resultant polymers had a compromised dispersity ($Đ \sim 1.41$). Yuan *et al.* reported the copolymerization of a TPE-containing monomer with benzyl methacrylate using PDMA macro-chain-transfer agents combing RAFT and polymerization-induced self-assembly (PISA) in ethanol, in which the correlation of the AIE effect to the nanostructure of polymer assemblies was explored.[31]

Despite this elegant process, high temperatures and/or a relatively long time frame are routinely applied in aqueous RAFT polymerisation, potentially limiting their applications in biological science. The Haddleton group introduced a novel synthetic route to perform aqueous copper-mediated RDRP *via* the *in situ* formation of Cu containing catalysts exploiting the rapid disproportionation (<10 seconds) as an advantageous driving force.[32–34] ATRP in water has often been described as being problematic with a Cu/tris(2-pyridylmethyl)amine (TPMA) complex being described as being the best and most versatile catalyst to employ in water[35] even though the quite popular Me_6Tren has been shown to be efficient.[32–34] This rapid rate of polymerization requires a high radical concentration at any moment in time, however, the excellent control we were seeking is often thought to require a low concentration of radicals, which is somewhat contradictory. Ballard and Asua have described how this apparent contradiction can be explained by taking into account radical diffusion time which explains this rapid and efficient polymerization.[36] We decided to use the route we had previously developed using Me_6Tren as this proved convenient and effective comforted with the explanation provided by Ballard and Asua. This strategy paves the way for the design and synthesis of an array of hydrophilic polyacrylamides and polyacrylates at sub-ambient temperatures with full monomer conversions producing polymers with narrow dispersities ($Đ < 1.10$) attained in just few minutes.[26,37] In addition, high end-group fidelity is retained even at high conversions, thereby allowing *in situ* chain extensions and multiblock copolymerizations by iterative monomer addition if required.[38] This chemistry was further demonstrated to be compatible with multiple functional groups and biologically associated media such as blood serum[39] and PBS.[32] Although aqueous Cu-RDRP has been proven to be robust and rapid, there is no report concerning the synthesis of water-soluble polymers with AIE features to date. It is noted that although certain "heavy metals" are often undesirable copper(II) is an essential part of a healthy diet with multiple copper containing enzymes present in the human body and has GRAS (generally regarded as safe) status from the FDA. In addition, copper salts can be easily removed using water swellable complexing resins if required.

Fluorescent organic nanoparticles (NPs) have drawn broad attention in bioluminescence imaging, due to their ready operation, low cost, as well as non-invasive and fast imaging.[40] Combining the AIE effect with organic NPs leads to the construction of high-performance fluorescent nanoparticles with excellent biocompatibility and photostability regarding biomedical applications.[41–43] It will be even more favourable if the AIE-active NPs could be instinctively generated driven by self-assembly of water-soluble polymers with AIE occurring in water, avoiding often tedious and time-consuming encapsulation of small organic components.

In previous work, the AIEgen-containing initiator tetraphenylethene bromoisobutyrate (TPEBIB) had been synthesized and employed to prepare a range of both hydrophobic and hydrophilic polyacrylates with AIE properties through Cu-wire mediated RDRP in varying organic solvents.[44] Herein, we present the synthesis of water-soluble AIE-active polymers with diverse architectures initiated by TPEBIB *via* aqueous Cu-mediated RDRP at sub-ambient temperatures (Scheme 1).

Results and discussion

Optimization of aqueous Cu-RDRP conditions of HEAM (DP = 100) initiated by TPEBIB

Initially, in order to examine the ability of the hydrophobic TPEBIB to initiate polymerization in aqueous media, aqueous Cu-RDRP of poly((ethylene glycol) methyl ethyl acrylate) ($PEGA_{480}$) was conducted in a vial with DMSO/water (3 : 1)

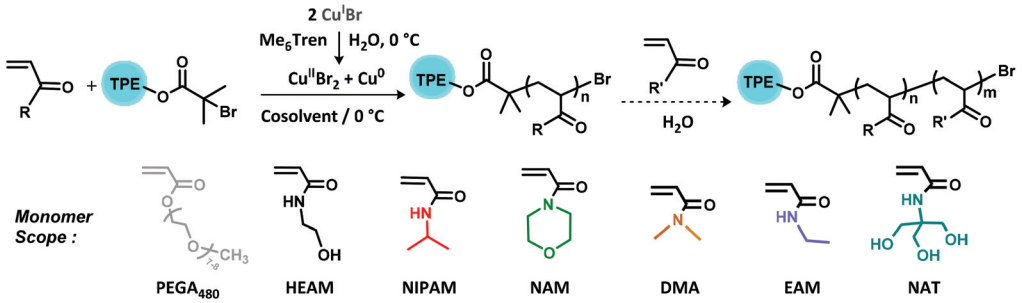

Scheme 1 Reaction scheme for homopolymerizations and *in situ* block copolymerizations of acrylamides and PEGA$_{480}$ with initiator TPEBIB in aqueous Cu-RDRP at 0 °C.

solvent, following the conditions developed in a previous report ([I] : [PEGA$_{480}$] : [Cu(I)Br] : [Me$_6$Tren] = 1 : 20 : 0.4 : 0.4).[32] The cosolvent was introduced in order to enhance the solubility of the hydrophobic initiator in the reaction media independently of the disproportionation of copper(I) in pure water as this is a much more rapid reaction than that in mixed water/organic solvents. Thus, it is noted that the catalyst is prepared by *in situ* disproportionation of Cu(I)Br/Me$_6$TREN in pure water at 0 °C prior to the addition of the monomer/co-solvent mixture is important and a requirement for effective polymerisation (Scheme 1); when organic cosolvents are used the equilibrium constant shifts markedly towards comproportionation as opposed to disproportionation of Cu(I). Pleasingly, the monomer conversion of PEGA$_{480}$ reached 98% in 20 h, resulting in a final polymer with M_n = 8900 g mol^{-1} with a dispersity = 1.11 (Fig. S1†). Considering these promising results with TPEBIB as initiator, the analogous polymerization of *N*-hydroxyethyl acrylamide (HEAM) targeting a moderate DP = 100 was attempted. However, surprisingly only 15% monomer conversion was achieved after 20 h (Table 1, entry 1). Thus, other cosolvents were applied to the binary system (Table 1, entries 2–5). Amongst them, THF and dioxane, with lower polarity of 0.207 and 0.164 respectively, showed much better performance than that of the more polar cosolvents DMSO, DMF and MeCN (0.444, 0.386, and 0.460).[45] The cosolvents with lower polarity (THF and dioxane) tended to be better solvents for the solubilisation of TPEBIB. The widely used alcoholic media previously used in aqueous Cu-RDRP,[46,47] were not explored in this work due to their limited solubility of TPEBIB in these solvents.

Although the monomer conversions increased significantly (>50%) by using THF or dioxane as the cosolvents, it is still not an ideal system due to the long reaction time required to reach high monomer conversion (20 h). In order to increase the polymerization rate, the concentration of the ligand with respect to the Cu(I)Br was increased with THF or dioxane as the cosolvent (Table 1, entries 6–9). Indeed, the increased [Me$_6$TREN] contributes to a higher conversion in a shorter time (Table 1, entries 6, 7 *vs.* 4; entries 8, 9 *vs.* 5). When [CuBr] : [Me$_6$TREN] = 0.8 : 0.8, monomer conversion of 88% (THF/water, 3 h) and 96% (dioxane/water, 4 h) were attained, with slightly broader molecular weight distributions ($Đ$ = 1.21 and 1.14, respectively) (entries 7 and 9). The higher $Đ$ values were attributed to relatively less effective deactivation due to the lower concentration of additional copper(II) halides, nevertheless, these dispersities were seen as being acceptable. An attempt using a higher copper-to-ligand ratio corresponding to the initiator (1.0 : 1.0) failed to speed the reaction or yield a more controlled polymer (Table 1, entry 10). Taking both the dispersity and polymerization rate into account, dioxane was chosen as the desired cosolvent with a [CuBr] : [Me$_6$TREN] = 0.8 : 0.8 for further polymerisations. Since the equilibrium constant (the balance between active and dormant species) is considerably higher in water than that in less polar organic solvents,[48] the volume ratio of dioxane to water was further reduced from 3 : 1 to 1 : 1 (Table 1, entry 11). As expected, the polymerization was significantly faster, attaining 99% monomer conversion in 1 h. Remarkably, the dispersity was as low as 1.08 under these conditions. Thus the conditions of

Table 1 Optimization of polymerization conditions of aqueous Cu-RDRP of *N*-hydroxyethyl acrylamide using the hydrophobic TPEBIB initiator

Entry[a]	Cosolvent[b]	Cu(I) : L	Time (h)	Con.[c] (%)	$M_{n,SEC}$[d] (g mol^{-1})	$Đ$
1	DMSO	0.8 : 0.4	20	15	10 200	1.24
2	DMF	0.8 : 0.4	20	9	1600	1.08
3	MeCN	0.8 : 0.4	20	26	6500	1.12
4	THF	0.8 : 0.4	20	61	16 700	1.12
5	Dioxane	0.8 : 0.4	20	51	12 000	1.11
6	THF	0.8 : 0.6	3	81	21 000	1.15
7	THF	0.8 : 0.8	3	88	26 500	1.21
8	Dioxane	0.8 : 0.6	4	83	20 400	1.11
9	Dioxane	0.8 : 0.8	4	96	23 100	1.14
10	Dioxane	1.0 : 1.0	3	94	24 700	1.15
11[e]	Dioxane	0.8 : 0.8	1	99	17 500	1.08

[a] In all reactions, the *in situ* disproportionation was conducted in 1 ml H_2O in an ice bath (0 °C). The total volume of the organic-water solution = 4 ml. [DP$_n$] : [TPEBIB] : [Cu(I)Br] : [Me$_6$Tren] = 100 : 1 : 0.8 : 0.4/0.6/0.8. [b] Cosolvent: dimethyl sulfoxide (DMSO), dimethylformamide (DMF), acetonitrile (MeCN), tetrahydrofuran (THF). 3 ml cosolvent was used for entries 1–10. 2 ml dioxane was used for entry 11. [c] Conversions were calculated according to ^{1}H NMR in DMSO-d^6. [d] Determined by SEC employing DMF as eluent calibrated by narrow PMMA molecular weight standards. [e] The volume ratio of dioxane to water is 1 : 1.

aqueous Cu-RDRP of *N*-hydroxyethyl acrylamide using hydrophobic TPEBIB initiator were optimized to be [TPEBIB] : [CuBr] : [Me_6TREN] = 1 : 0.8 : 0.8 in dioxane/water (1 : 1) binary mixture, which were applied to all the remaining polymerizations (otherwise stated) in this work.

Aqueous homopolymerizations: monomer scope, kinetic analysis, and varying DPs

In addition to HEAM, other commercial hydrophilic monomers, including *N*-isopropylacrylamide (NIPAM), 4-acryloylmorpholine (NAM), *N*,*N*-dimethylacrylamide (DMA), *N*-ethylacrylamide (EAM) and *N*-[tris(hydroxymethyl)methyl] acrylamide (NAT) were also successfully polymerized targeting DP = 100 under identical optimized conditions (Fig. 1A–F). Homopolymerizations of these various monomers reached full monomer conversion (≥99%) within 1–2 h. The monomodal mass distribution, narrow dispersities ($Đ$ = 1.08–1.15), as well as the excellent correlation between the theoretical ($M_{n,th}$) and the experimental molecular weights ($M_{n,NMR}$ and $M_{n,SEC}$), collectively indicated good controlled/living characteristics of this chemistry. This is in accordance with the explanation put forward by Ballard and Asua.[36]

The purified polymers were also characterized by NMR (Fig. S2 and S3†) and FT-IR (Fig. S4†) to investigate the different architectures. The attachment of the TPE group to polymers was exhibited by the signals δ = 7.15–6.77 ppm in ^{1}H NMR spectrum, δ = 150–120 ppm of ^{13}C NMR spectrum, together with the overlapping traces of the RI and UV (λ_{ex} = 309 nm) in the SEC (Fig. S5†). Additionally, the characteristic peaks of the side chains were assigned (Fig. S2–S4†).

In order to further demonstrate the effectiveness of the system and the polymerization rate, kinetic investigations were conducted for the homopolymerizations of HEAM and NIPAM (Fig. S6† and Fig. 2A, B). The results revealed near-100% monomer conversions in <1 hour (95% in 30 min for HEAM and 98% in 45 min for NIPAM). It is highlighted that ln([M]$_0$/[M$_t$]) increased linearly with respect to the reaction time in the dioxane/water media, indicating the polymerization rate to be first order in monomer concentration. This is quite remarkable compared with the wholly aqueous system, where achieving linear first-order kinetics proved challenging due to the extremely fast reaction.[34,37] Furthermore, a linear dependence of molecular weight with respect to monomer conversion (Fig. 2B) and low dispersity values ($Đ$ ~ 1.10) during the reac-

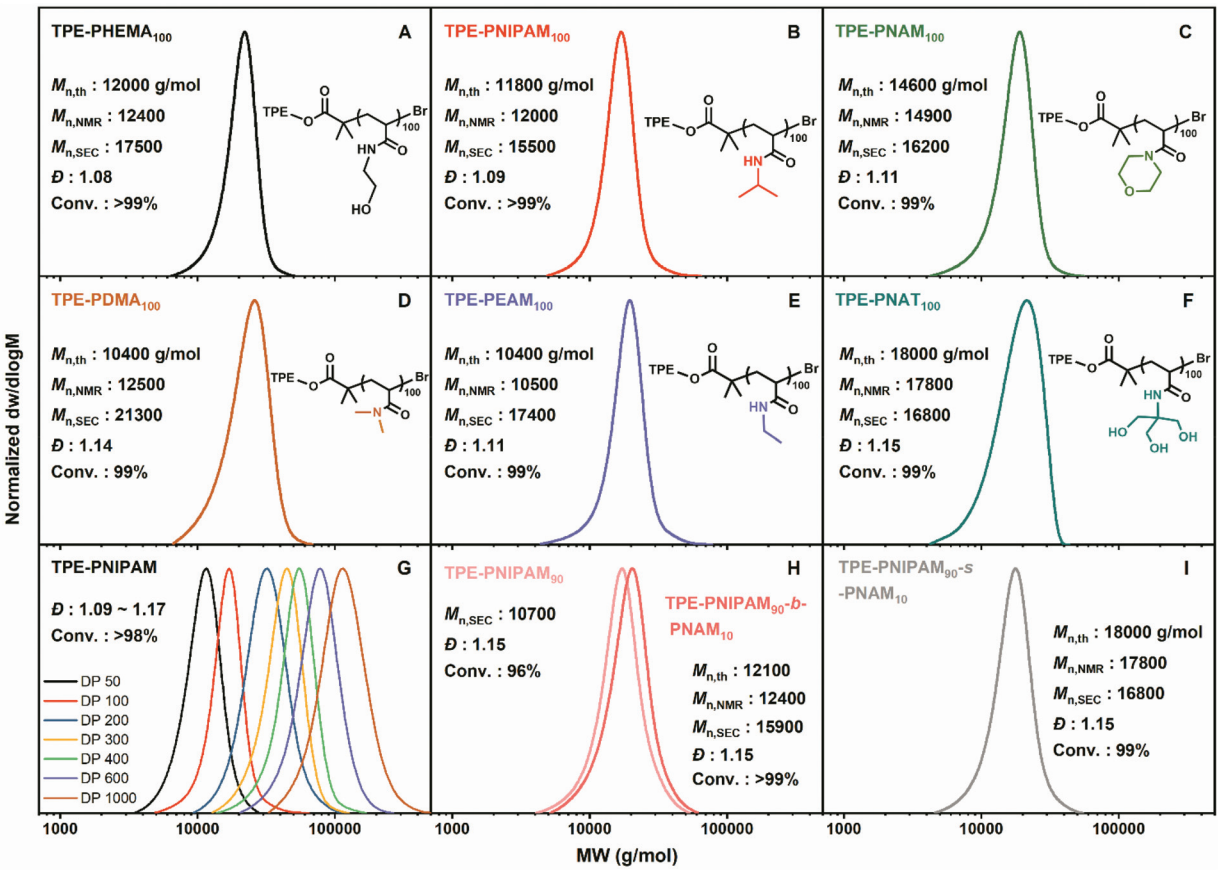

Fig. 1 DMF-SEC molecular weight distribution of synthesized TPE-terminated polyacrylamides. (A) TPE-PHEAM$_{100}$, (B) TPE-PNIPAM$_{100}$, (C) TPE-PNAM$_{100}$, (D) TPE-PDMA$_{100}$, (E) TPE-PEAM$_{100}$, (F) TPE-PNAT$_{100}$, (G) TPE-PNIPAM with targeted DP = 50–1000, (H) *in situ* block copolymerization by sequential monomer addition; TPE-PNIPAM$_{90}$ (light pink) and TPE-PNIPAM$_{90}$-*b*-PNAM$_{10}$ (pink), (I) statistical polymerization of TPE-PNIPAM$_{90}$-*s*-PNAM$_{10}$.

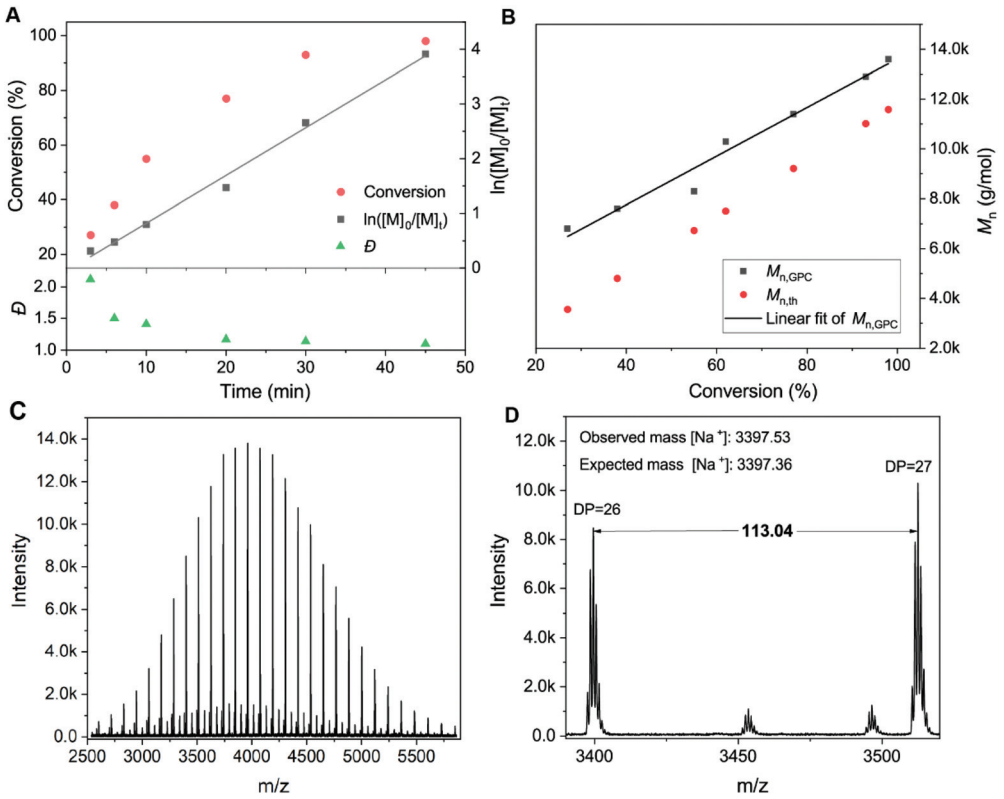

Fig. 2 (A) Kinetic study of aqueous Cu-RDRP of TPE-PNIPAM$_{100}$; (B) comparison of $M_{n,GPC}$ and theoretical molecular weights. (C and D) MALDI-ToF-MS spectra of TPE-PNIPAM$_{25}$ synthesized *via* Cu-RDRP in aqueous solution.

tion also verified that the polymerizations proceed in a well-controlled manner. Matrix assisted laser desorption–ionization time-of-flight mass spectrometry (MALDI-ToF-MS) revealed the presence of the TPE end group with a repeating unit of mass 113.04, corresponding to NIPAM (Fig. 2C and D).

With an increasing interest in thermally responsive polymer assemblies, the homopolymerization of NIPAM targeting differing molecular weights (DP = 50–1000) was attempted to probe the potential of aqueous Cu-RDRP initiated by TPEBIB to give thermoresponsive polymers with AIE properties for use in sensor applications (Fig. 1G and Table S1†). It has been reported that it can be important to optimise the copper-to-ligand ratio when targeting different DPs to afford the most well-defined polymers using aqueous RDRP.[32,37,48] Significantly, in this present study, all polymerizations proceeded to near quantitative conversions (≥98%) without further optimizing this reagent ratio, and were well-controlled with a dispersity of 1.09–1.17 within 1 or 2 h even when DP was as high as 1000 (M_n = 114 kDa). Symmetrical monomodal shifts were evidently observed from the SEC traces (Fig. 1G), indicative of excellent control when high molecular weights were targeted.

Block and statistical copolymerizations of PNIPAM and PNAM

In order to obtain AIE polymers with high end group fidelity, *in situ* chain extensions from PNIPAM were carried out using sequential monomer addition. Copolymerization of PNIPAM and PNAM has been reported to be somewhat problematic with limited conversion of the second PNAM block (56%) due to chain termination events preventing efficient product formation.[49] However, we decided to revisit this monomer pair especially as NAM has been less explored using copper-mediated RDRP than that in the case of RAFT. The total DP was fixed at 100 with a change in molar ratio for a series of block copolymers. NIPAM (targeted DP = 50, 70, 80, 90, and 95) was firstly polymerized employing the previous conditions, sampled after 35 min, prior to the second aliquot of deoxygenated NAM in aqueous solution being injected into the reaction vial. Samples were taken again after 40 min. For comparison, the statistical copolymerization experiments were also carried out by adding the mixture of both monomers at the beginning of polymerization.

For the block copolymers (PNIPAM-*b*-PNMA), the conversion of both the first and second block was ≥95% (Table 2). SEC analysis revealed monomodal peaks with a shift of the mass distribution to higher molecular weights upon the second block addition whist maintaining narrow dispersities ($Đ \sim 1.15$) (Fig. 1H and Fig. S7†), indicative of full reaction of PNIPAM chains with additional NAM, thus suggesting excellent end group fidelity at high monomer conversions. Of the statistical copolymers (PNIPAM-*s*-PNMA), total monomer conversion reached ≥98% within 1 or 2 h, yielding polymers with

Table 2 *In situ* block copolymerization and statistical copolymerization by aqueous Cu-mediated RDRP initiated by TPEBIB

Copolymers[a]	Con.[b] (%)	$M_{n,th}$ (g mol^{-1})	$M_{n,SEC}$ [c] (g mol^{-1})	$M_{n,NMR}$ (g mol^{-1})	$Đ$
TPE-PNIPAM$_{95}$-*b*-PNAM$_5$	>99 (99)	12 000	16 000	12 300	1.15
TPE-PNIPAM$_{90}$-*b*-PNAM$_{10}$	>99 (96)	12 100	15 900	12 400	1.15
TPE-PNIPAM$_{80}$-*b*-PNAM$_{20}$	>99 (97)	12 400	16 500	12 700	1.16
TPE-PNIPAM$_{70}$-*b*-PNAM$_{30}$	99 (98)	12 700	16 900	13 600	1.17
TPE-PNIPAM$_{50}$-*b*-PNAM$_{50}$	96 (95)	13 200	17 400	14 000	1.15
TPE-PNIPAM$_{95}$-*s*-PNAM$_5$	98	12 000	15 700	12 300	1.14
TPE-PNIPAM$_{90}$-*s*-PNAM$_{10}$	99	12 100	15 700	12 500	1.12
TPE-PNIPAM$_{80}$-*s*-PNAM$_{20}$	98	12 400	15 400	12 500	1.17
TPE-PNIPAM$_{70}$-*s*-PNAM$_{30}$	99	12 700	14 500	12 800	1.15
TPE-PNIPAM$_{50}$-*s*-PNAM$_{50}$	>99	13 200	16 500	13 400	1.11

[a] Copolymerization was conducted using the conditions [TPEBIB] : [CuBr] : [Me$_6$TREN] = 1 : 0.8 : 0.8 in dioxane/water (1 : 1) binary mixture. Expect TPE-PNIPAM$_{50}$-*s*-PNAM$_{50}$ (2 h), the other statistical copolymerizations were stopped in 1 h. [b] Conversions were calculated according to ^{1}H NMR in CD_3OD; the values in the brackets are the conventions of the first block. [c] Determined by SEC employing DMF as eluent calibrated by narrow PMMA molecular weight standards.

low molecular weight distributions ($Đ$ = 1.11–1.17) (Table 2, Fig. 1I and S8†). In all cases, the negligible deviation between the theoretical ($M_{n,th}$) and experimental molecular weights (especially $M_{n,th}$) (Table 2) as well as monomodal SEC traces without tailing (Fig. S7 and S8†) was demonstrated. Chemical compositions were characterized by NMR and FT-IR (Fig. S2–S4†).

In addition, the thermal properties of the obtained polymers were characterized by thermogravimetric analysis (TGA) and differential scanning calorimetry (DSC) measurements (Fig. S9 and S10†). The hydroxyl-containing polymers, TPE-PHEAM$_{100}$ and TPE-PNAT$_{100}$, showed two degradation stages with a decomposition temperature (T_d) at 5% weight loss under nitrogen at 292 °C and 253 °C, respectively. The other polymers all had one degradation stage, losing 5 wt% at temperatures ranging between 383 and 409 °C. DSC analysis demonstrated the glass transition temperature (T_g) of these polyacrylamides was in the range of 126–168 °C, of which TPE-PNAM$_{100}$ had the highest T_g. With the increase of DP from 50 to 1000, the T_g of homopolymer TPE-PNIPAM increased from 140 °C to 149 °C. Moreover, when increasing the ratio of PNAM from 0% to 50%, the T_g of block copolymers and statistical copolymers increased from 143 °C to 146 °C and 153 °C, respectively.

Thermoresponsivity of TPE-PNIPAM containing polymers: LCST, aggregate size and morphology

The thermoresponsive properties of the TPE-terminated PNIPAM homopolymers and copolymers were initially studied using UV-vis and dynamic light scattering (DLS). It was found that the transmission of the block copolymer aqueous solution and the corresponding particle size was dynamically changing due to dynamic self-assembly, as exemplified by TPE-PNIPAM$_{90}$-*b*-PNAM$_{10}$ (Fig. S11†). With an increase in the stabilization time, the transmittance of polymer solution at high temperatures increased from 20% to 80% and smaller aggregates were detected. There was no real change observed after being left for 1 day at ambient temperature. Consequently, to ensure the comparability of the data, all samples were left in water at ambient temperature for 1 day prior to measurements.

Herein, the cloud point (T_{cp}) is defined here by the temperature at which a 10% sharp loss in sample transmittance is detected in the heating cycle. The T_{cp} of homopolymer TPE-PNIPAM (DP = 50) = 34 °C, which is not affected by the DP from 50 (34.3 °C) to 1000 (34.8 °C) (Fig. S12†). Interestingly, by changing the end group of PNIPAM$_{100}$ from TPEBIB to ethyl α-bromoisobutyrate (EBiB, less hydrophobic/aggregating), the cloud point increased to 39.0 °C (Fig. S12†). Furthermore, the T_{cp} of EBiB-terminated PNIPAM has a much larger dependence on the DP, decreasing from 43.6 °C to 35.6 °C with an increase in DP from 50 to 400. Thus, there seems to be a significant contribution of the hydrophobic end-moiety (TPE) in the self-assembly behaviour of these AIE polymers in aqueous media.

In order to construct thermoresponsive particles at physiologically temperatures, a hydrophilic comonomer (NAM) was incorporated by both block and statistical copolymerization. The effects of the different copolymerization methods, as well as the comonomer ratio on the LCST, were evaluated (Fig. 3A and B). In the block copolymers (Fig. 3A), there was a distinctly reduced loss of transmittance with an increasing ratio of NAM at elevated temperatures. The T_{cp} increased to 35.9 °C and 37.1 °C with 5 mol% and 10 mol% NAM, respectively. It was difficult to define the T_{cp} when the block incorporation ratio of NAM ≥20 mol%, without rapid loss in transmittance. Conversely, all statistical copolymers showed low transmittance (<10%) upon heating, with a linearly increasing T_{cp} up to 45.1 °C as a function of the DP values of NAM (Fig. 3B and Fig. S13†). The cooling cycles were also recorded for all the polymers, exhibiting similar hysteresis (~4 °C lower than T_{cp}) in full transmittance recovery (Fig. S12 and 13†).

The particle size information was collected as a function of temperature (30–70 °C) by DLS (Fig. 3C and Fig. S14†). At low temperatures (<LCST), the hydrodynamic diameter (D_h) of all the TPE-PNIPAM containing polymers in aqueous solutions is approximately 30 nm with a polydispersity (PDI) of ~0.25, due to the self-assembly driven exclusively by the hydrophobic end moiety. When the temperature approaches T_{cp} upon heating,

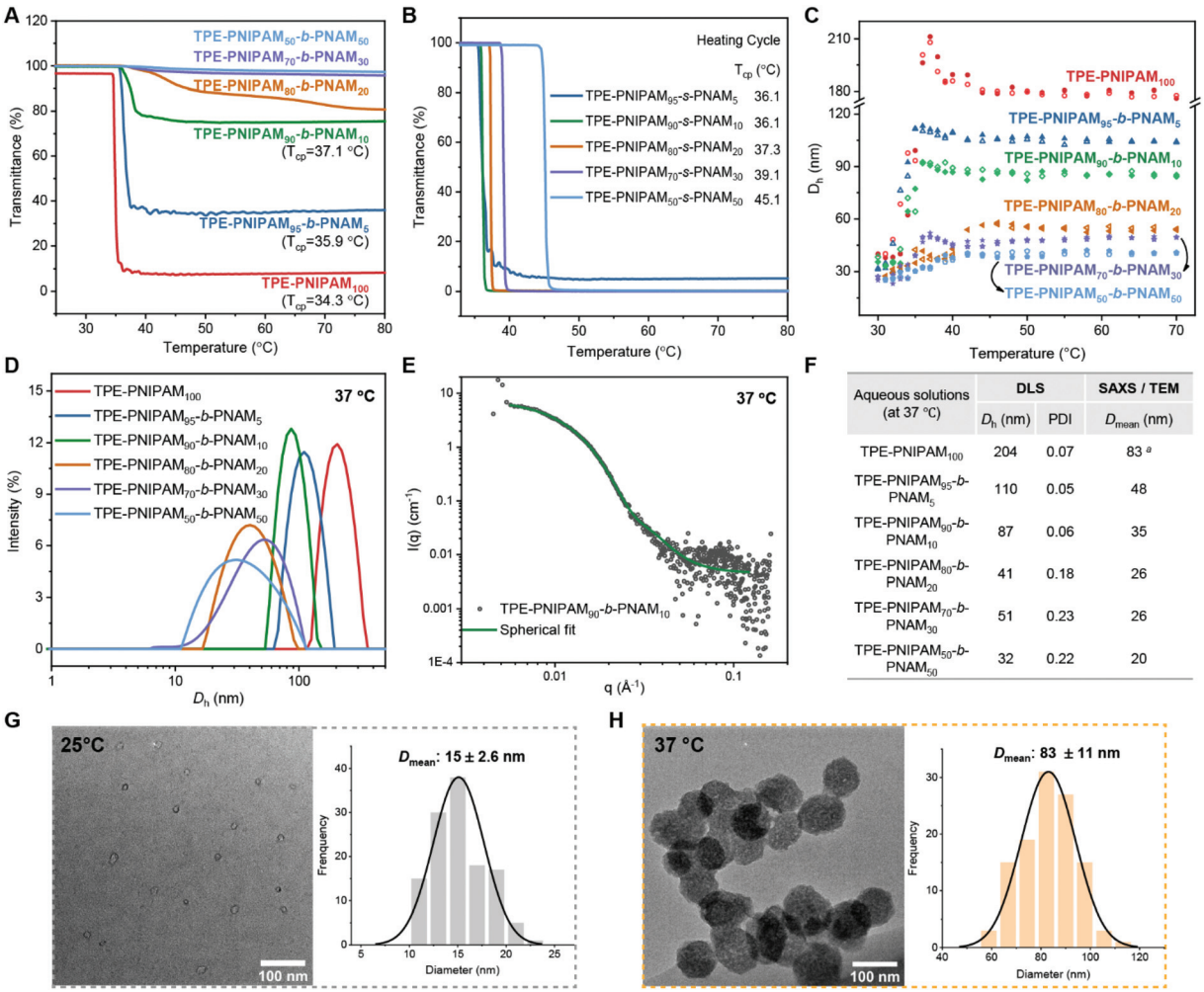

Aqueous solutions (at 37 °C)	DLS		SAXS / TEM
	D_h (nm)	PDI	D_{mean} (nm)
TPE-PNIPAM$_{100}$	204	0.07	83 [a]
TPE-PNIPAM$_{95}$-*b*-PNAM$_5$	110	0.05	48
TPE-PNIPAM$_{90}$-*b*-PNAM$_{10}$	87	0.06	35
TPE-PNIPAM$_{80}$-*b*-PNAM$_{20}$	41	0.18	26
TPE-PNIPAM$_{70}$-*b*-PNAM$_{30}$	51	0.23	26
TPE-PNIPAM$_{50}$-*b*-PNAM$_{50}$	32	0.22	20

Fig. 3 Cloud point curves upon heating of TPE-PNIPAM$_{100}$ and block copolymers (A) and statistical copolymers (B) with a heating rate of 1 °C min^{-1}. (C) The hydrodynamic diameters of block copolymers as a function of temperature. Solid symbols for heating cycle and hollow symbols for cooling cycle. (D) The particle size distribution by intensity of TPE-PNIPAM$_{100}$ and block copolymers at 37 °C. (E) Characterization of particle morphology of aqueous solution of TPE-PNIPAM$_{90}$-*b*-PNAM$_{10}$ at 37 °C by SAXS. (F) The comparison of particle sizes determined by DLS and SAXS or TEM. [a] Determined by TEM and the others determined by SAXS. The particle morphology and size histograms characterized by TEM at 25 °C (G) and 37 °C (H) of TPE-PNIPAM$_{100}$. Histograms are from $n > 100$. All the samples were stabilized in water for 1 day before measurements. [Polymer] = 500 μM for SAXS and [polymer] = 100 μM for the other characterizations.

all the block copolymers tend to self assembles into larger aggregates with a narrower population distribution (Fig. S15†). Increasing the NAM molar ratio from 0 to 50% in the block polymers contributes to decreases in stabilized particle sizes at high temperatures, with D_h varying from 180 nm to 40 nm. By comparison, the reverse trend was found for statistical copolymers (D_h = 240–1600 nm) (Fig. S14†).

Particle behaviour in aqueous solutions at 37 °C were further compared using different techniques (Fig. 3D–H). In terms of TPE-PNIPAM$_{100}$, TPE-PNIPAM$_{95}$-*b*-PNAM$_5$ and TPE-PNIPAM$_{90}$-*b*-PNAM$_{10}$, whose $T_{cp} \leq 37.1$ °C, the D_h values were 204 nm, 110 nm, and 87 nm, respectively (Fig. 3D and F). It is noteworthy distributions (PDI = 0.05–0.07). For the other block copolymers, the D_h = 31–42 nm with a broader dispersity (PDI = 0.18–0.23). Small-angle X-ray scattering (SAXS) was also used (Fig. 3E and Fig. S16†). The mean diameter (D_{mean}) determined by SAXS is approximately half that obtained from DLS (Fig. 3F). This is as SAXS and transmission electron microscopy (TEM) typically only reflect the internal core or physical diameter, despite which, D_h also includes the thickness of an electrical dipole layer adhered that they all self-assembled to form particles with quite narrow to its surface.[50] Additionally, as exemplified by TPE-PNIPAM$_{90}$-*b*-PNAM$_{10}$ (Fig. 3E), all of the particles of TPE-PNIPAM$_{100}$ and the block copolymers were fitted to be a spherical modal by SAXS (Fig. S16†). TEM was applied with sample preparation at 25 °C ($<T_{cp}$) and 37 °C ($>T_{cp}$), respectively so as to visualize the changes of the particle size and morphology as a function of temperature. The spherical particles experienced a coil-to-globule transition with a swelling (from 15 nm to 83 nm) due to chain collapse and aggregation of the PNIPAM (Fig. 3G, H and Fig. S17†).

Photophysical properties

As a typical aggregation-induced emission luminogen (AIEgen), TPE shows no emission when fully dissolved but becomes highly luminescent in the aggregated state.[51] It was the target that these TPE-terminated polymers would be fluorescent in a wholly aqueous solution. Their UV-vis absorption spectra recorded in water displayed a maximum absorption band at 306–312 nm arisen from the TPE group (Fig. S18†). Subsequently, the photoluminescence (PL) spectra of the homopolymers with different concentrations (0.01–1 mg mL^{-1}) in an aqueous solution at room temperature were measured. The emission intensity was proportional to [polymer] (Fig. 4A, B and Fig. S19†). Taking TPE-$PNIPAM_{100}$ as an example, distinct emission was observed when the polymer concentration >0.1 mg mL^{-1} (Fig. 4A). The emissive performance of these 6 homopolymers was compared, among which TPE-$PNIPAM_{100}$ shows the most intense emission efficiency followed by TPE-$PNAM_{100}$. Contact angle measurements were used to investigate the structure–property relationship of the spin-coated films of these homopolymers (Fig. 4C). It was found that the water-soluble polyacrylamides, which are more hydrophobic (larger contact angle), were better emitters in aqueous solution, ascribed to aggregation of the TPE groups. The emission of the polymers in media with a variation in water fraction (f_w) of THF/water mixtures were measured (Fig. 4D and Fig. S20†). As exemplified by TPE-$PNIPAM_{90}$-*b*-$PNAM_{10}$, the emission was extremely weak at f_w < 60%, which was greatly enhanced at f_w = 90% and reached the maximum at a 99% water content, 250-fold higher than that in pure THF solution.

We subsequently investigated how the emission intensity changed as a function of solution temperatures in the range of 20 to 50 °C (Fig. 4E and F). The non-thermoresponsive polymer TPE-$PNAM_{100}$ was also included for comparison, which had a liner emission decrease trend by gradually elevating the temperature (Fig. 4F). By contrast, in the cases of TPE-PNIPAM-based copolymers, a minor emission decrease was observed between 30 °C and T_{cp}, attributing to the increasing hydrophobicity on a basis of integral hydrophilicity caused by gradual dehydration of the PNIPAM chains. Moreover, the fluorescence intensity dropped sharply (~15%) from T_{cp} to T_{cp} +1 for TPE-$PNIPAM_{100}$ and TPE-$PNIPAM_{95}$-*b*-$PNAM_5$ aqueous solutions, which is indistinct for the other block copolymers (Fig. 4F). The difference results from the fact that it is more difficult for the UV excitation beam to reach TPE moiety buried in the larger micelles after the coil-to-globule transmission.[52] Statistical copolymers also behaved in a similar fashion (Fig. S21†).

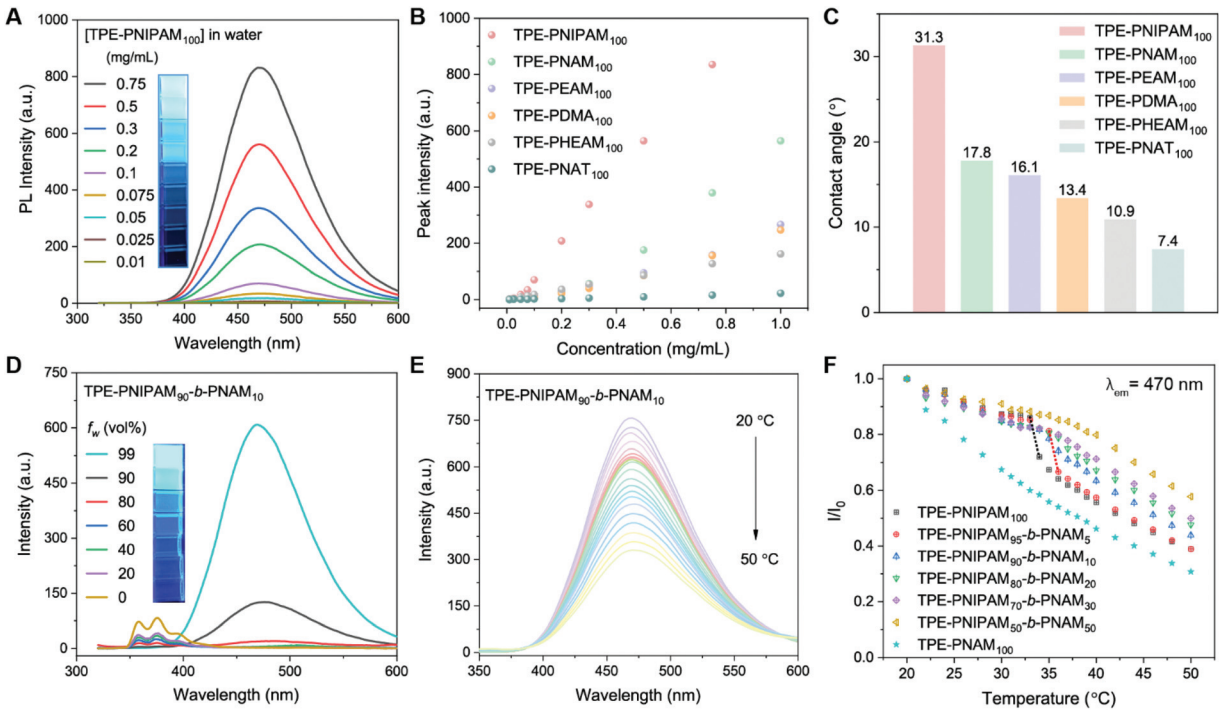

Fig. 4 The PL spectra of TPE-$PNAM_{100}$ (A) and the peak intensity of the PL spectra (λ_{em} = 470 nm) of different TPE-terminated homopolymers (B) in water as a function of concentration at 20 °C. (C) The contact angle of various homopolymers' film. (D) The PL spectra of TPE-$PNIPAM_{90}$-*b*-$PNAM_{10}$ in water–THF mixtures with different water fractions (f_w) measured at 20 °C with [polymer] = 50 μM. The PL spectra of TPE-$PNIPAM_{90}$-*b*-$PNAM_{10}$ (E) and the peak intensity of the PL spectra (λ_{em} = 470 nm) of different block copolymers (F) in water as a function of temperature (I is the PL intensity at the corresponding temperature; I_0 is emission intensity at 20 °C. [Polymer] = 50 μM). λ_{ex} = 310 nm for all the measurements. The inserted pictures in (A) and (D) were taken under a UV lamp (λ = 302 nm).

Cell imaging

Based on these results, TPE-PNIPAM$_{90}$-*b*-PNAM$_{10}$ with a suitable nanoparticle size in water at physiological temperature (D_h = 87 nm and D_{mean} = 35 nm measured by DLS and SAXS, respectively) as well as excellent aggregate-state fluorescent was selected to explore the application in cell imaging. The cytotoxicity of TPE-PNIPAM$_{90}$-*b*-PNAM$_{10}$ was first evaluated by a 3-(4,5-dimethyl-2-thiazolyl)-2,5-diphenyltetrazolium bromide (MTT) cell viability assay using 4T1 cells as the model (Fig. 5A). The cell viability retained >95% at a polymer concentration of up to 30 μg mL^{-1}, indicating excellent biocompatibility of TPE-PNIPAM$_{90}$-*b*-PNAM$_{10}$ with living cells. Subsequently, the cell staining capability of TPE-PNIPAM$_{90}$-*b*-PNAM$_{10}$ was assessed using a confocal laser scanning microscope (CLSM) (Fig. 5B). Bright blue fluorescence within cells was observed after incubation with 10 μg mL^{-1} polymer for 3 h. The co-localization experiment was further conducted upon co-staining 4T1 cells with LysoTracker Red (LTR), a commercial lysosome imaging dye. The results showed that the staining regions of LTR overlapped well with those of TPE-PNIPAM$_{90}$-*b*-PNAM$_{10}$. The Pearson's correlation coefficient was calculated to be 0.85 (Fig. S22†), suggesting the good lysosome-targeting capability of TPE-PNIPAM$_{90}$-*b*-PNAM$_{10}$. Furthermore, the photostability of the polymer was quantitatively compared with LTR (Fig. 5C). After 60 scans with continuous irradiation (λ_{ex} = 405 nm), the emission intensity of TPE-PNIPAM$_{90}$-*b*-PNAM$_{10}$ retained over 70% of its initial value, whereas LTR suffered a significant signal loss with only 20% remaining intensity, strongly indicative of the superior photostability of TPE-PNIPAM$_{90}$-*b*-PNAM$_{10}$ to commercial dyes. Evidently, with its low cytotoxicity, high specificity and good photo-bleaching resistance, TPE-PNIPAM$_{90}$-*b*-PNAM$_{10}$ is a promising candidate functioning as lysosome-specific fluorescent probes for bioimaging.

Conclusions

In summary, various acrylamides, including NIPAM, were polymerized within 1 or 2 h in a near quantitative fashion, with excellent control over chain lengths (DP = 50–1000) and molecular weight distributions ($Đ$ = 1.08–1.17). The polymerisations show good linear first order kinetics and successful *in situ* block copolymerizations are possible. A library of thermoresponsive block and statistical copolymers with TPE terminus were obtained, which were demonstrated to possess varying lower critical solution temperature (LCST) and particle sizes depending on the compositions and copolymerization methods. Moreover, all the TPE-labelled polymers were shown to be AIE-active and the photo-physical properties exhibited dependence on the polymer concentration, side chain, as well as temperature. TPE-PNIPAM$_{90}$-*b*-PNAM$_{10}$, spontaneously self-assembled into fluorescent NPs with a suitable size at physiological conditions, was exemplified to be applicable for lysosome-specific cell imaging owing to its low cytotoxicity, high specificity and good photostability. By changing the compositions and copolymerization method of the TPE-PNIPAM-based polymers, fluorescent thermoresponsive nanoparticles with tuneable sizes were straightforwardly formed by self-assembly in aqueous media without any encapsulation. The emission intensity was regulated by the hydrophobicity of the polymers as well as their concentration and the temperature of an aqueous solution. Significantly, the PNIPAM-containing polymers possessed better fluorescent performance and

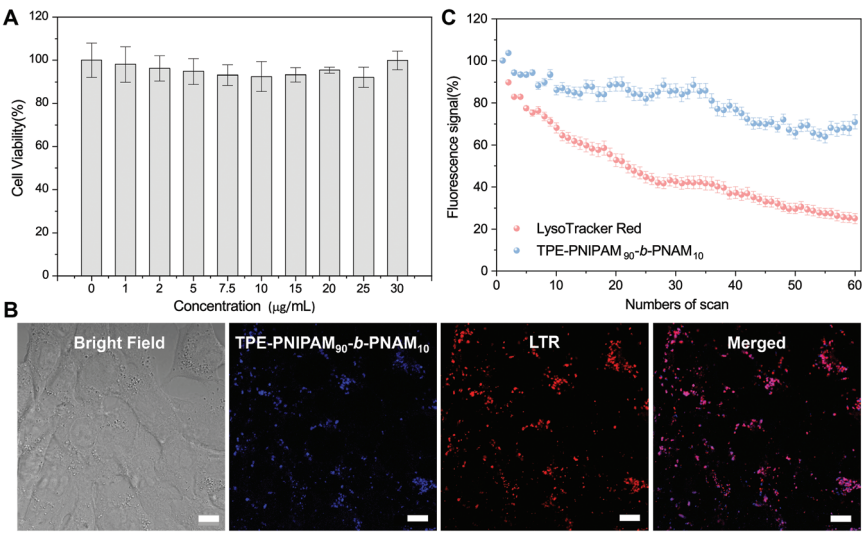

Fig. 5 (A) The cytotoxicity of TPE-PNIPAM$_{90}$-*b*-PNAM$_{10}$ to 4T1 cells incubated with different polymer concentrations. (B) Bright field and confocal images of 4T1 cells stained with TPE-PNIPAM$_{90}$-*b*-PNAM$_{10}$ (10 μg mL^{-1}, 3 h), LysoTracker Red (LTR, 1 μM, 30 min) and the merged image. λ_{ex}: 405 nm (polymer) and 561 nm (LTR); emission filter: 400–600 nm (polymer) and 620–700 nm (LTR). Scale bar = 10 μm. (C) Loss in fluorescence of 4T1 cells stained respectively with TPE-PNIPAM$_{90}$-*b*-PNAM$_{10}$ and LTR as a function of the numbers of the scan of laser irradiation.

resisted the thermo-induced emission reduction. The good biocompatibility and photostability of these emissive nanoparticles were exemplified by TPE-PNIPAM$_{90}$-*b*-PNAM$_{10}$, indicating their potential for lysosome-specific bioimaging application.

Author contributions

CM and DH designed the experiments, CM conducted all of the synthesis and most of the characterizations and wrote the draft manuscript. TH and NN conducted the cell imaging experiments. LA conducted the MALDI measurements and helped with data analysis. SE helped the discussions and purification of polymers. DL offered the instrument trainings and expertise, especially with regard to SEC analysis. SH performed the SAXS measurements and analysis. DH supervised the project and made corrections of the manuscript.

Conflicts of interest

There are no conflicts to declare.

Acknowledgements

We are grateful for financial support from University of Warwick and China Scholarship Council. We are grateful for the Research Technology Platforms (RTP) in University of Warwick, especially Daniel Lester, James Town and Ivan Prokes for providing NMR, SEC, FT-IR, UV-Vis, DSC, DLS, TGA, SAXS, TEM training and equipment. We also acknowledge the collaboration which was funded by the National Natural Science Foundation of China (21905176) and the Science and Technology Plan of Shenzhen (JCYJ20190808142403590).

Notes and references

1 J. Luo, Z. Xie, J. W. Y. Lam, L. Cheng, H. Chen, C. Qiu, H. S. Kwok, X. Zhan, Y. Liu, D. Zhu and B. Z. Tang, *Chem. Commun.*, 2001, 1740–1741, DOI: 10.1039/B105159H.
2 Z. Zhao, J. W. Y. Lam and B. Z. Tang, *J. Mater. Chem.*, 2012, **22**, 23726–23740.
3 W. W. H. Lee, Z. Zhao, Y. Cai, Z. Xu, Y. Yu, Y. Xiong, R. T. K. Kwok, Y. Chen, N. L. C. Leung, D. Ma, J. W. Y. Lam, A. Qin and B. Z. Tang, *Chem. Sci.*, 2018, **9**, 6118–6125.
4 W. Qin, Z. Yang, Y. Jiang, J. W. Y. Lam, G. Liang, H. S. Kwok and B. Z. Tang, *Chem. Mater.*, 2015, **27**, 3892–3901.
5 M. Gao and B. Z. Tang, *ACS Sens.*, 2017, **2**, 1382–1399.
6 Y.-l. Liu, Z.-k. Wang, W. Qin, Q.-l. Hu and B. Z. Tang, *Chin. J. Polym. Sci.*, 2017, **35**, 365–371.
7 T. Lin, X. Su, K. Wang, M. Li, H. Guo, L. Liu, B. Zou, Y.-M. Zhang, Y. Liu and S. X.-A. Zhang, *Mater. Chem. Front.*, 2019, **3**, 1052–1061.
8 J.-S. Ni, P. Zhang, T. Jiang, Y. Chen, H. Su, D. Wang, Z.-Q. Yu, R. T. K. Kwok, Z. Zhao, J. W. Y. Lam and B. Z. Tang, *Adv. Mater.*, 2018, **30**, 1805220.
9 D. Mao, W. Wu, S. Ji, C. Chen, F. Hu, D. Kong, D. Ding and B. Liu, *Chem*, 2017, **3**, 991–1007.
10 G. Qi, F. Hu, L. Shi, M. Wu and B. Liu, *Angew. Chem.*, 2019, **131**, 16375–16381.
11 Y. Wang, W. Wu, J. Liu, P. N. Manghnani, F. Hu, D. Ma, C. Teh, B. Wang and B. Liu, *ACS Nano*, 2019, **13**, 6879–6890.
12 X. Cai and B. Liu, *Angew. Chem., Int. Ed.*, 2020, **59**, 9868–9886.
13 J. Mei, N. L. Leung, R. T. Kwok, J. W. Lam and B. Z. Tang, *Chem. Rev.*, 2015, **115**, 11718–11940.
14 T. Han, Z. Yao, Z. Qiu, Z. Zhao, K. Wu, J. Wang, A. W. Poon, J. W. Y. Lam and B. Z. Tang, *Nat. Commun.*, 2019, **10**, 5483.
15 T. Han, H. Q. Deng, Z. J. Qiu, Z. Zhao, H. K. Zhang, H. Zou, N. L. C. Leung, G. G. Shan, M. R. J. Elsegood, J. W. Y. Lam and B. Tang, *J. Am. Chem. Soc.*, 2018, **140**, 5588–5598.
16 R. Hu, A. Qin and B. Z. Tang, *Prog. Polym. Sci.*, 2020, **100**, 101176.
17 Z. Qiu, X. Liu, J. W. Lam and B. Z. Tang, *Macromol. Rapid Commun.*, 2019, **40**, 1800568.
18 H. Ma, C. Qi, C. Cheng, Z. Yang, H. Cao, Z. Yang, J. Tong, X. Yao and Z. Lei, *ACS Appl. Mater. Interfaces*, 2016, **8**, 8341–8348.
19 R. Yang, Y. Wang, W. Luo, Y. Jin, Z. Zhang, C. Wu and N. Hadjichristidis, *Macromolecules*, 2019, **52**, 8793–8802.
20 Y. Liu, J. W. Y. Lam, X. Zheng, Q. Peng, R. T. K. Kwok, H. H. Y. Sung, I. D. Williams and B. Z. Tang, *Macromolecules*, 2016, **49**, 5817–5830.
21 Y. B. Hu, J. W. Y. Lam and B. Z. Tang, *Chin. J. Polym. Sci.*, 2019, **37**, 289–301.
22 S. Perrier, *Macromolecules*, 2017, **50**, 7433–7447.
23 T. G. McKenzie, E. Colombo, Q. Fu, M. Ashokkumar and G. G. Qiao, *Angew. Chem., Int. Ed.*, 2017, **56**, 12302–12306.
24 F. Lorandi, M. Fantin, Y. Wang, A. A. Isse, A. Gennaro and K. Matyjaszewski, *ACS Macro Lett.*, 2020, **9**, 693–699.
25 A. Anastasaki, V. Nikolaou, G. Nurumbetov, P. Wilson, K. Kempe, J. F. Quinn, T. P. Davis, M. R. Whittaker and D. M. Haddleton, *Chem. Rev.*, 2015, **116**, 835–877.
26 G. R. Jones, A. Anastasaki, R. Whitfield, N. Engelis, E. Liarou and D. M. Haddleton, *Angew. Chem., Int. Ed.*, 2018, **57**, 10468–10482.
27 N. Corrigan, K. Jung, G. Moad, C. J. Hawker, K. Matyjaszewski and C. Boyer, *Prog. Polym. Sci.*, 2020, **111**, 101311.
28 G. Gody, T. Maschmeyer, P. B. Zetterlund and S. Perrier, *Nat. Commun.*, 2013, **4**, 2505.
29 G. Gody, T. Maschmeyer, P. B. Zetterlund and S. Perrier, *Macromolecules*, 2014, **47**, 639–649.
30 Y. Zhao, Y. Wu, S. Chen, H. Deng and X. Zhu, *Macromolecules*, 2018, **51**, 5234–5244.
31 M. Huo, Q. Ye, H. Che, X. Wang, Y. Wei and J. Yuan, *Macromolecules*, 2017, **50**, 1126–1133.

32 Q. Zhang, P. Wilson, Z. Li, R. McHale, J. Godfrey, A. Anastasaki, C. Waldron and D. M. Haddleton, *J. Am. Chem. Soc.*, 2013, **135**, 7355–7363.
33 S. Efstathiou, A. M. Wemyss, G. Patias, L. Al-Shok, M. Grypioti, D. Coursari, C. Ma, C. J. Atkins, A. Shegiwal, C. Wan and D. M. Haddleton, *J. Mater. Chem. B*, 2021, **9**, 809–823.
34 E. Liarou, Y. Han, A. M. Sanchez, M. Walker and D. M. Haddleton, *Chem. Sci.*, 2020, **11**, 5257–5266.
35 M. Fantin, A. A. Isse, A. Gennaro and K. Matyjaszewski, *Macromolecules*, 2015, **48**, 6862–6875.
36 N. Ballard and J. M. Asua, *ACS Macro Lett.*, 2020, **9**, 190–196.
37 G. R. Jones, Z. Li, A. Anastasaki, D. J. Lloyd, P. Wilson, Q. Zhang and D. M. Haddleton, *Macromolecules*, 2016, **49**, 483–489.
38 F. Alsubaie, A. Anastasaki, P. Wilson and D. M. Haddleton, *Polym. Chem.*, 2015, **6**, 406–417.
39 Q. Zhang, Z. Li, P. Wilson and D. M. Haddleton, *Chem. Commun.*, 2013, **49**, 6608–6610.
40 J.-S. Ni, Y. Li, W. Yue, B. Liu and K. Li, *Theranostics*, 2020, **10**, 1923–1947.
41 W. Che, L. Zhang, Y. Li, D. Zhu, Z. Xie, G. Li, P. Zhang, Z. Su, C. Dou and B. Z. Tang, *Anal. Chem.*, 2019, **91**, 3467–3474.
42 Z. Zhao, C. Chen, W. Wu, F. Wang, L. Du, X. Zhang, Y. Xiong, X. He, Y. Cai and R. T. Kwok, *Nat. Commun.*, 2019, **10**, 1–11.
43 R. Zhang, G. Niu, Q. Lu, X. Huang, J. H. C. Chau, R. T. K. Kwok, X. Yu, M.-H. Li, J. W. Y. Lam and B. Z. Tang, *Chem. Sci.*, 2020, **11**, 7676–7684.
44 C. Ma, T. Han, M. Kang, E. Liarou, A. M. Wemyss, S. Efstathiou, B. Z. Tang and D. Haddleton, *ACS Macro Lett.*, 2020, **9**, 769–775.
45 C. Reichardt and T. Welton, *Solvents and solvent effects in organic chemistry*, John Wiley & Sons, 2011.
46 C. Waldron, Q. Zhang, Z. Li, V. Nikolaou, G. Nurumbetov, J. Godfrey, R. McHale, G. Yilmaz, R. K. Randev, M. Girault, K. McEwan, D. M. Haddleton, M. Droesbeke, A. J. Haddleton, P. Wilson, A. Simula, J. Collins, D. J. Lloyd, J. A. Burns, C. Summers, C. Houben, A. Anastasaki, M. Li, C. R. Becer, J. K. Kiviaho and N. Risangud, *Polym. Chem.*, 2014, **5**, 57–61.
47 Q. Zhang, P. Wilson, A. Anastasaki, R. McHale and D. M. Haddleton, *ACS Macro Lett.*, 2014, **3**, 491–495.
48 G. R. Jones, R. Whitfield, A. Anastasaki and D. M. Haddleton, *J. Am. Chem. Soc.*, 2016, **138**, 7346–7352.
49 A. Anastasaki, A. J. Haddleton, Q. Zhang, A. Simula, M. Droesbeke, P. Wilson and D. M. Haddleton, *Macromol. Rapid Commun.*, 2014, **35**, 965–970.
50 C. M. Maguire, M. Rösslein, P. Wick and A. Prina-Mello, *Sci. Technol. Adv. Mater.*, 2018, **19**, 732–745.
51 Y. Hong, J. W. Y. Lam and B. Z. Tang, *Chem. Commun.*, 2009, 4332–4353, DOI: 10.1039/B904665H.
52 L. Tang, J. K. Jin, A. Qin, W. Z. Yuan, Y. Mao, J. Mei, J. Z. Sun and B. Z. Tang, *Chem. Commun.*, 2009, 4974–4976, DOI: 10.1039/B907382E.

